Solidification Macrostructure of Compacted Graphite Cast Iron and its relationship with Shrinkage Porosity

M. López[1*], G. Rivera[1,2], J. Massone[1,2] and R. Boeri[1,2]
[1]Metallurgy Division, Faculty of Engineering, UNMdP, Mar del Plata, Argentina
[2]INTEMA, UNMdP – CONICET, Mar del Plata, Argentina

This work focuses on the study of the solidification macrostructure of compacted graphite iron and its relationship with shrinkage porosity formation. Cast samples especially developed to present shrinkage porosity were examined after applying the DAAS technique, which involves hot shake out of the castings at temperatures above the eutectoid, followed by an austempering. The samples were then sectioned, polished and etched with Nital 2%. The results were compared with those obtained earlier by Rivera et al on spheroidal and flake graphite cast irons. The results show that, similarly to spheroidal and flake graphite irons, the solidification of compacted graphite iron is dominated by the presence of relatively large grains of austenite that can be observed by the naked eye. Differences in the grain size were detected as a function of the position into the different volumes analyzed, observing a typical ingot structure. The dispersed shrinkage cavities formed were found inside the grains and located between the austenite dendrite arms.
The results allow the authors to propose a novel explanation of the solidification of compacted graphite irons that shares common features with spheroidal and lamellar graphite irons.

Keywords: solidification macrostructure, compacted graphite iron, DAAS technique, shrinkage porosity, solidification model.

Introduction

Compacted graphite cast irons are gaining increasing interest nowadays. Their main current applications include diesel engine blocks, turbo housings and exhaust manifolds for the automotive industry. Compacted graphite iron (CGI) is replacing lamellar graphite iron (LGI) in applications where greater mechanical strength is needed, as long as its lower thermal conductivity than flake graphite iron does not become a limiting factor. As the production of CGI is forecasted to increase over the next years, the basic understanding of its phase transformations becomes very important. Nowadays, the knowledge about the solidification behaviour of CGI is limited. The prediction and prevention of casting defects such as micro porosity demands a thorough understanding of the solidification of CGI.

Recent studies of the solidification micro and macrostructure of spheroidal graphite cast iron (SGI) carried out by Rivera et al[1,2] have provided new experimental results that gave support to an explanation of the solidification of eutectic SGI. This explanation postulates that each solidification unit is a grain of eutectic austenite that has a dendritic substructure and contains a very large number of graphite nodules.

Rivera et al[3,4,5] stated that in free graphite cast irons the process of solidification starts with an independent nucleation of austenite dendrites and graphite from the melt. As heat is extracted, austenite dendrites grow and interact with graphite precipitates. They claim that this interaction is quite different depending on the graphite morphology.

Flake graphite and austenite grow cooperatively with both phases in contact with the melt. Otherwise in SGI, spheroidal graphite particles are enveloped by an austenite layer soon after they get in contact with the growing austenite dendrites, and further growth of graphite is controlled by the diffusion of carbon from the melt to the graphite through the austenite shell. These authors proposed the term "eutectic colony" to describe the shapes formed during the solidification of free graphite irons.

In the case of CGI, a big step in the study of its solidification mechanism was carried out by Mampaey[6], who presented samples quenched during solidification which show that some of the compacted graphite particle tips remain in direct contact with the melt. Now it is important to complete this understanding by employing the new techniques and knowledge developed.

The objective of this investigation is to reveal and to characterise the macrostructure of compacted graphite iron in order to develop a theory explaining how solidification proceeds in compacted graphite cast irons and to correlate the solidification structure with shrinkage porosity, similarly as Elmquist et al made for LGI[7].

Experimental Procedure

All tests were carried out on samples especially designed to develop large and small shrinkage cavities. They were designed employing dimensions and geometric relationships that violate the basic design rules. The conditions that,

* Corresponding author, email: marcosl@fi.mdp.edu.ar

according to Campbell[8], give the most difficult feeding conditions were used, such as: right angles, hot spots, intricate areas, section changes, metallostatic low pressure zones, long feeders, thin sections, etc. The system was then simulated employing the software MagmaSoft, in order to make the necessary modifications in the geometry to maintain the presence of shrinkage porosity in the model.

The simulations were performed employing the properties of an eutectic ductile iron GJS-600 listed in the database of Magmasoft with the following characteristic temperatures:

- Liquidus temperature: 1169ºC
- Solidus temperature: 1166ºC

The parameters that were adopted to hold the simulations are as follow:

- Pouring temperature: 1360ºC
- Pouring time: 5 s
- Feeding efficiency: 70%
- Inoculation treatment: 70%
- Graphite precipitation: 7

Regarding to the mould material, Silica_dry sand at a temperature of 25ºC was used. It was also employed a uniform meshing along the whole moulding cavity with 200.000 elements.

Concluded this process the design showed in Fig. 1was reached.

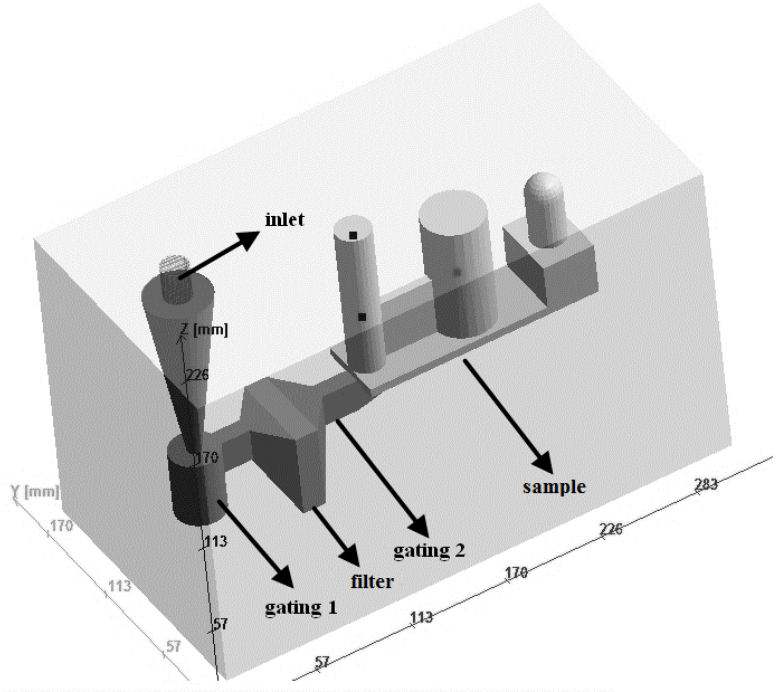

Fig. 1: 3D view of the model.

Fig. 2 indicates the velocity distribution after 2.65 seconds from pouring, showing that the velocity inside the piece is lower than the critical value of 1 m/s, avoiding turbulent flow.

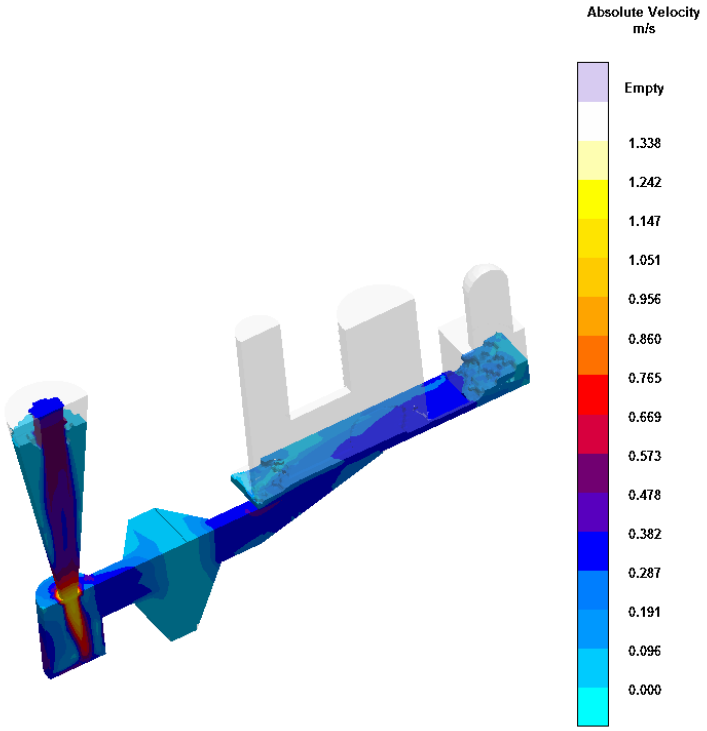

Fig. 2: Velocity distribution in the final design after 2.65 s.

Fig. 3 shows the temperature at the middle section of the mould cavity when the cavitie is completelly filled (5 seconds after pouring started). It can be observed that the minimum temperature in the piece is 1230 °C, which is higher than the liquidus temperature (1169 °C) .

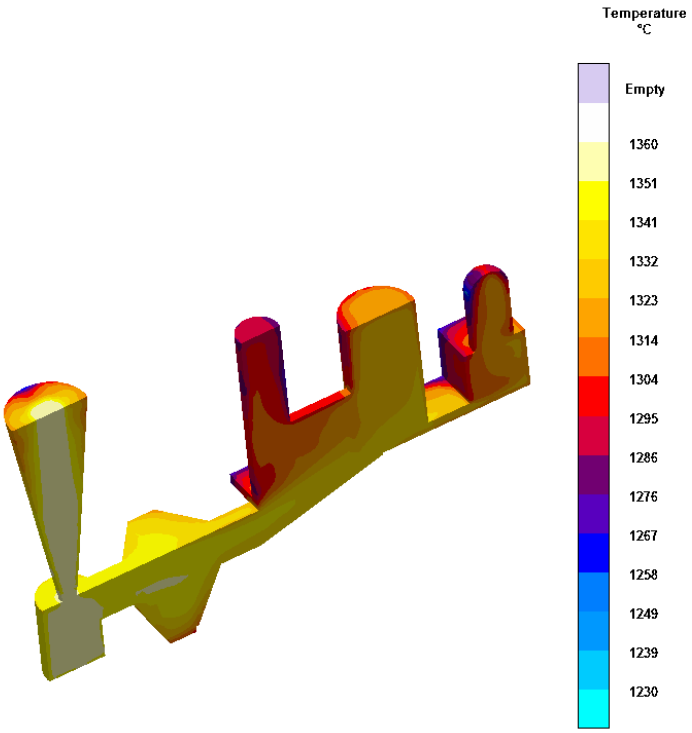

Fig. 3: Pouring temperature of the final design.

Lastly, Fig. 4 shows the porosity distribution at the middle section of the part predicted by the software once solidification has finished. Through this prediction, it can be confirmed the presence of shrinkage porosity in the experimental sample.

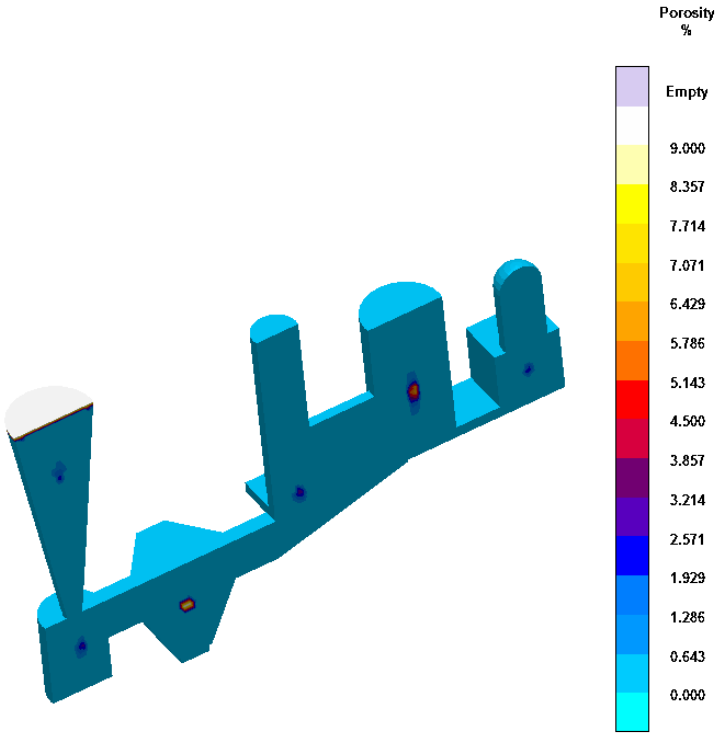

Fig. 4: Porosity at the middle section of the final design.

Once the final design was completed employing MagmaSoft, experimental meltings were carried out by using a medium frecuency induction furnace of 50 kg capacity at the foundry laboratory of INTEMA. The chemichal compositions of the heats are listed in Table 1. Melt A, with a CE of 4.29%, has eutectic composition, while Melt B is hypereutectic. The melts were nodularised by using between 0.6 and 0.67 wt-% of Fe-Si-Mg-Ca-Ce (6 wt-%Mg), and post inoculated with 0.5 wt-% of Fe-Si (80 wt-%Si). Compositions include small amounts of Cu and Ni that were added to reach the level of austemperability needed to carry out the DAAS procedure.

Table 1: Chemical Compositions.

Melt	% C	% Si	% Mn	% S	% P	% Mg	% Cu	% Ni
A	3.38	2.74	0.17	0.017	0.033	0.020	0.97	0.66
B	3.53	3.15	0.18	0.016	0.041	0.015	1.025	0.78

After the moulds were filled, the cast parts were shaken out when their minimum temperature reached approximately 950ºC, being then transferred to a furnace held at 920ºC, where they were kept during 30 min in order to allow their temperature homogenisation. The parts were then austempered in a molten salt bath held at 360ºC for 90 min. This relatively high austempering temperature was chosen in order to maximize the amount of retained austenite.
Later the samples were sectioned, polished and etched with Nital 2%. Nodularity was measured by comparison with standard charts.

Results and Discussion

Fig. 5 shows the graphite morphology obtained in both melts. These micrographies reveal that samples of Melt A show a nodularity of 30%, whereas samples of Melt B have a nodularity of 15%. These values were found from the average of five different fields analysed and are consistent with the amounts of Mg found in each melt.

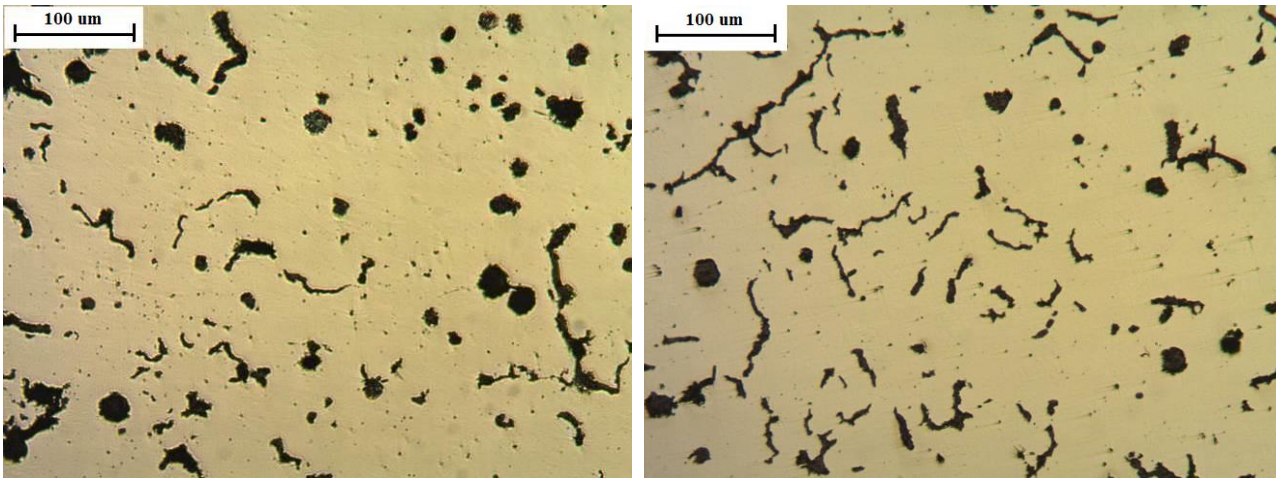

Fig. 5: Microstructure of Melt A (left) and Melt B (right). Unetched.

The microstructure of the metallic matrix after Nital 2% etching is shown in Fig. 6. The austempering heat treatment lead to a matrix microstructure formed by a fine mixture of acicular ferrite and austenite. This austenite is in fact the primary austenite, which has been retained in the matrix after the use of the DAAS technique.

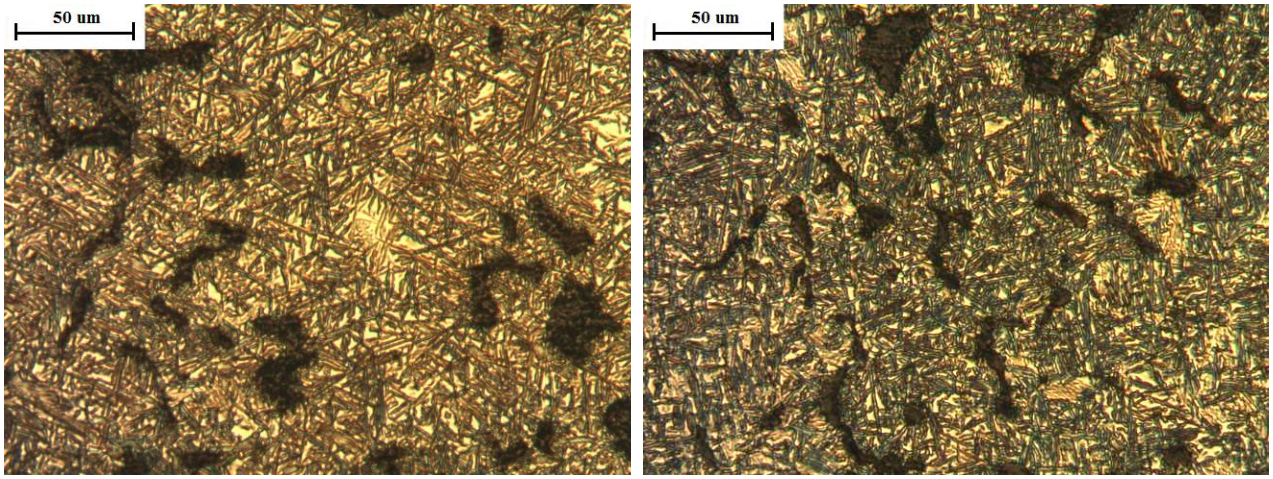

Fig. 6: Microstructure of Melt A (left) and Melt B (right) after etching with Nital 2%.

The retained austenite kept the crystalline orientation defined during solidification. Therefore, after standard chemical etching, the grained structure of the austenite can be observed macrographically. Fig. 7 and Fig. 8 show the macrostructures obtained after applying DAAS technique and etching with Nital 2% for Melts A and B respectively. These are some of the first pictures published to date in which the solidification macrostructure of CGI is simultaneously shown with shrinkage porosity. Small equiaxed grains are visible at the faster solidifying portions of the sample, while much larger, and sometimes columnar, grains are observed on other areas of the samples.

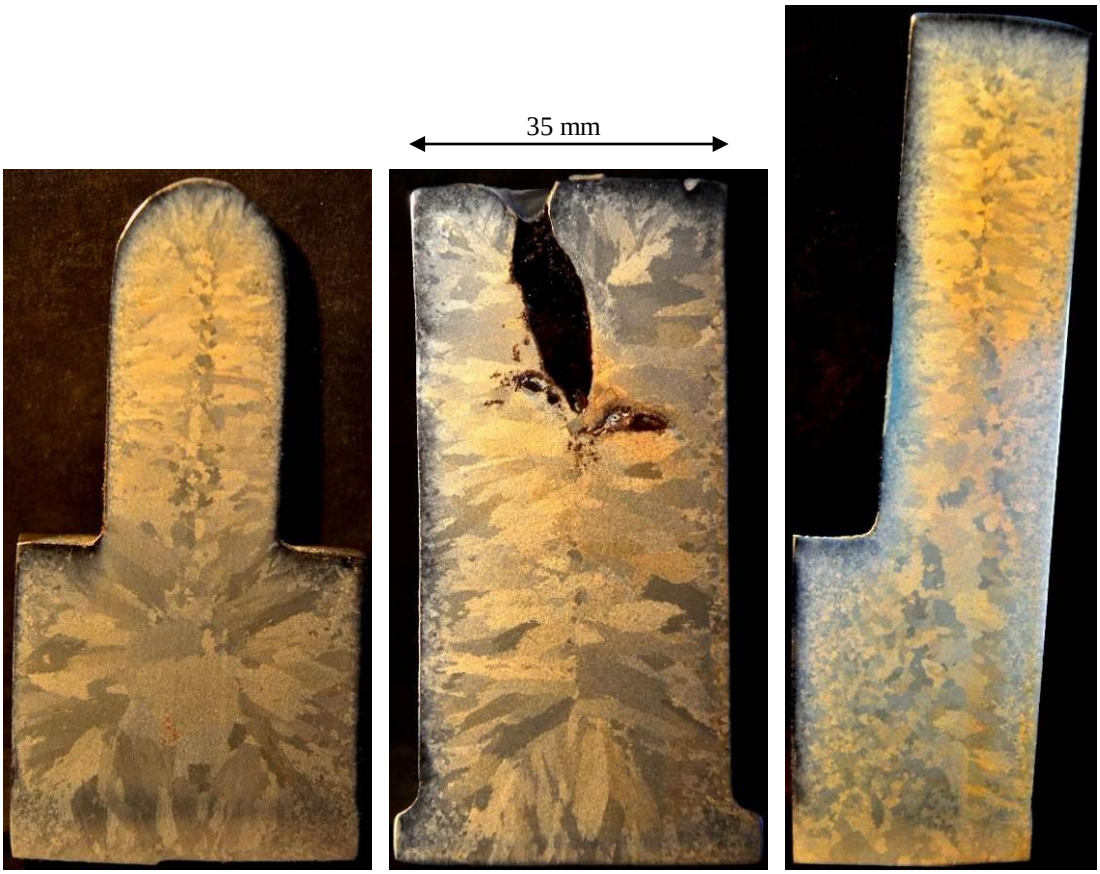

Fig. 7: Solidification macrostructures obtained for Melt A.

Fig. 8: Solidification macrostructures obtained for Melt B.

When comparing the results shown in Fig. 7 and Fig. 8 with those obtained previously by Rivera et al[3] for SGI and LGI, the similarity of CGI macrostructure is noticeable. Just as it was concluded earlier for SGI and LGI, the solidification of CGI is strongly dominated by the nucleation and growth of relatively large grains of austenite, each one including a large number of graphite particles. The use of EBSD by Rivera et al[3] for samples of SGI and LGI demonstrated that there is a clear correlation between the results obtained applying DAAS technique and EBSD analysis. EBSD technique proved that austenite grains can be properly observed by employing the procedure DAAS.

Based on the observation of the macrostructure and the previous experience exposed in the references[1-5], it is proposed that the solidification of CGI proceeds in a manner similar to that characteristic of LGI. The nucleation and growth of austenite and graphite proceed mostly independently in the melt. Austenite grows dendritically. The portions of the casting exposed to higher cooling rates reach larger undercoolings and show a relatively large density of austenite nucleae, resulting in small grain size. On the other hand, slower cooling portions show smaller density of austenite nucleae and therefore larger grain size. The graphite particles grow in the melt, most probably as spheroids during the first stages, but later, as the growing austenite dendrites collide with them, form eutectic colonies in which austenite and graphite grow cooperatively, with both phases in contact with the melt.

Concerning the location of porosity, Fig. 9 shows that dispersed shrinkage cavities from samples obtained in this research are mostly intragranular and locate between austenite dendrite arms. It can also be observed that there is no a linear arrangement of shrinkage porosity, as would be found if cavities were formed between the austenite grains.

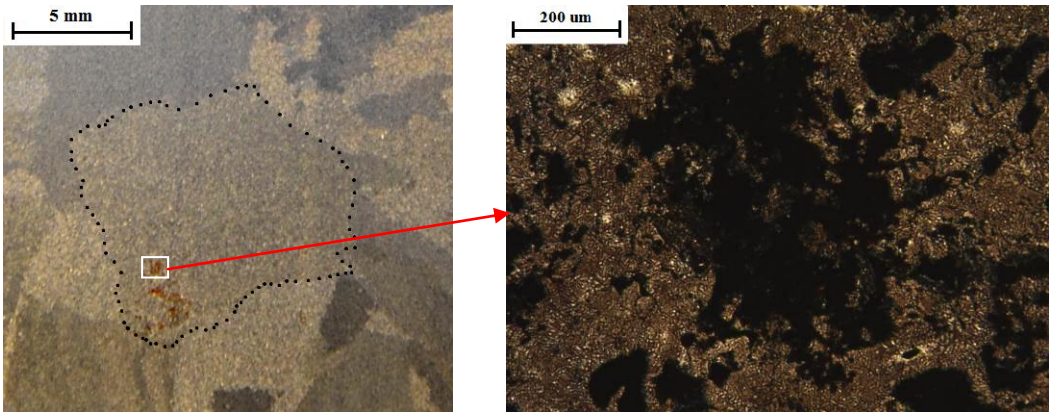

Fig. 9: Porosity in macro and microstructure.

The main features of the solidification of CGI revealed by this investigation are quite important for practical aspects. Nowadays, the computational packages aimed at the prediction of the filling and solidification of free graphite cast irons poured in moulds do not take into account the actual size and shape of the austenite dendrites, to the best of our knowledge. The prediction of fluid flow, filling, temperature evolution and defect formation should be improved by the adoption of more realistic solidification models.

Conclusions

1. The solidification of compacted graphite iron is dominated by the presence of relatively large grains of austenite that, after the use of the DAAS technique, can be observed by the naked eye, just as it was previously demonstrated for lamellar and spheroidal graphite cast irons. It is proposed that the solidification of CGI proceeds in a manner similar to that of LGI, this is with an independent nucleation and growth of austenite and graphite from the melt.
2. The dispersed shrinkage cavities form mostly inside the grains, and locate between the austenite dendrite arms.

Acknowledgements

This study made use of an academic license of MagmaSoft, which is gratefully acknowledged.

References

1. G. Rivera, R. Boeri and J. Sikora: 'Revealing and characterising solidification structure of ductile cast iron', *Materials Science and Technology*, June 2002, Vol. 18, 691-697.
2. G. Rivera, R. Boeri and J. Sikora: 'Research Advances in Ductile Iron Solidification', *AFS Transactions*, Vol. 111, 3-159, pp 1-11 (2003)
3. G. Rivera, P. R. Calvillo, R. Boeri, Y. Houbaert and J. Sikora*:* 'Examination of the solidification macrostructure of spheroidal and flake graphite cast irons using DAAS and ESBD', *Materials Characterization 59*, 2008, 1342-1348.

4. G. Rivera, R. Boeri, J. Sikora: 'Searching for a Unified Explanation of the Solidification of Cast Irons', *Eighth International Symposium on Science and Processing of Cast Iron*, Beijing, China, 2006, Vol 1. pp 45-50.
5. G. Rivera, R.Boeri, J. Sikora: 'Growth of eutectic austenite in free graphite cast irons', *Key Engineering Materials 457*, pp 67-72 (2011).
6. F. Mampaey: 'Influence of compacted graphite on solidification morphology of cast iron', *AFS Transactions*, 2000, Vol. 27, 11-17.
7. L. Elmquist and A. Diószegi: 'Shrinkage porosity and its relation to solidification structure of grey cast iron parts', *International Journal of Cast Metals Research*, 2010, Vol. 23, 44-50.
8. Campbell, J: 'Castings', Butterworth-Heinemann Ltd, Chapters 2 and 5. 1991.